JAERI-M
6034

MULTIPLE SCATTERING OF NEUTRONS IMPINGING ON THICK MATERIALS IN THE RESONANCE ENERGY REGION

March 1975

Makio OHKUBO

日本原子力研究所
Japan Atomic Energy Research Institute

この報告書は，日本原子力研究所が JAERI-M レポートとして，不定期に刊行している研究報告書です．入手，複製などのお問合わせは，日本原子力研究所技術情報部（茨城県那珂郡東海村）あて，お申しこしください．

JAERI-M reports, issued irregularly, describe the results of research works carried out in JAERI. Inquiries about the availability of reports and their reproduction should be addressed to Division of Technical Information, Japan Atomic Energy Research Institute, Tokai-mura, Naka-gun, Ibaraki-ken, Japan.

JAERI-M 6034

Multiple Scattering of Neutrons Impinging on Thick Materials in the Resonance Energy Region

Makio OHKUBO

Division of Physics, Tokai, JAERI

(Received February 10, 1975)

A multiple scattering effect on neutron capture and scattering yields was measured for tungsten plates of several thicknesses in the resonance energy region with a ^{6}Li - ^{7}Li pair glass scintillator. Observed capture and scattering data were compared with the results obtained by the Monte-Carlo calculations. At resonance energies, the capture yields show peaks for thin samples, whereas they show dips for thick samples. The reason for these complicated features are interpreted by investigating the distributions of neutron path length in the samples. A new method of $\Gamma n/\Gamma$ determination, which is essentially insensitive to the sample thickness, is discussed.

共鳴領域に於る厚い試料に入射する中性子の多重散乱

日本原子力研究所東海研究所物理部
大久保　牧　夫

（１９７５年２月１０日受理）

中性子共鳴領域での多重散乱の影響を調べるために，タングステンの補獲，散乱各イールドを，$L_i^6-L_i^7$ グラスシンチレータを用いて，リニアックの中性子飛行時間スペクトロメータで測定した。一方，モンテカルロ法プログラムを作成し，試料中の中性子の振舞のシミレーションを行い，補獲，散乱イールドを計算した。計算値と実験値の比較では，かなりよい一致を得た。

実験及び計算によると，共鳴エネルギーに於る補獲イールドは，試料が薄いときはピークをなし，試料を厚くしていくと逆にディプになる。この飽和現象を中性子が試料中で補獲されるまでに動く行路程の分析から解明した。

また飽和補獲率の値から Γ_n/Γ の値を推定する新しい方法を議論した。

目　次　な　し

Multiple Scattering of Neutrons Impinging on Thick Materials in the Resonance Energy Region

1. Introduction

When a neutron impinges on a thick material, it is multiply sacttered until either it escapes from the surface of the materials or it is captured in the material. Effects of the multiple scattering are too complicate to be estimated quantitatively, especially when the energy of the incident neutron is in the resonance energy region.[1] In the field of nuclear engineering, thick materials are often used, where multiple scattering effects play an essencial role in viewpoint of neutron transport problem. In some computor program for resonance analyses, multiple scattering effect is calculated by the Monte-Carlo method as a correction for finite sample thicknesses,[2] because the energy dependences of the microscopic cross sections of the target nuclei are appreciably different from those of the capture and scattering probabilities for samples of finite thicknesses. In spite of practical importance, the quantitative study of these problems leaves untouched. So it is nessesary to make an effort to investigate into the multiple scattering effects in thick materials in the resonance energy region.

In this paper the results of the capture and scattering yields measurements on tungsten plates of several thicknesses are described. Experimental data obtained by the time of flight spectrometer at JAERI linac are compared with the value calculated by a Monte-Carlo program "MCRTOF" in which neutron paths in the materials are simulated taking into accounts the microscopic cross sections of the target nuclei. These calculations were made also for resonances in cobalt (132 eV) and silver (5.2 eV). At resonance energies, the capture probability

of a neutron shows peaks for thin samples, whereas it shows dips for thick samples. The scattering probability of a neutron from the incident surface shows peaks for thin samples, whereas for thick samples it shows dips at higher side of the resonance energies. These phenomena are reasonably understood from the distributions of path length of the neutron until it is captured in the sample. Dependences of the capture and scattering probabilities on the resonance parameters and the recoil energy were examined.

At a resonance energy, a relation is found between the ratio $\Gamma n/\Gamma$ and the value of capture probability for sufficiently thick samples.

2. Instrumentations and Measurements

Neutron scattering and capture yields for thick tungsten paltes were measured at the 47-m station of the time of flight facilities of the JAERI-linac.[3] Details of the facilities were reported eleswhere,[4] and only a brief descriptions are made in the following. Figure 1 shows a schematic figure of the TOF facilities. Neutrons were produced in a water cooled tantalum target bombarded with nominal 120 MeV electron beam, and were moderated in a boron-paraffin block. Neutrons passed through evacuated aluminum flight tubes of 30 cm diameter, and were collimated by a number of lead and paraffin collimaters to have a cross section of 6 cm diameter at the sample position. The neutron flight path length was 47.07 m from the neutron source to the center of the sample. Scattered neutrons and capture gamma rays from the samples were detected by a pair of ^{6}Li and ^{7}Li glass scintillators as shown in fig. 2. The center line of the two scintillators was perpendicular to the incident neutron beam. By the ^{6}Li glass scintillator scattered neutrons and capture gamma rays were detected, whereas only capture gamma rays by the ^{7}Li glass scintillator. By suitable adjustment of pulse height discrimination levels for these detectors, scattered neutron yields were obtained as the difference between these for the two

scintillators in simultaneous mode of measurements, provided that the solid angle subtended by the detectors at the sample, and capture gamma ray self shielding factor were identical for the two detectors. Gamma ray subtraction method was essentially the same as that of Asgher and Brooks.[5] The scintillators and the neutron beam tube were shielded by boron-paraffin wax and lead, the inner surface of which was lined with B_4C layer. The scattering samples were inclined at 45 degrees with the incident beam. The ^6Li glass scintillator (NE908) used for detection of scattered neutrons had $4\frac{3}{8}$" diameter and $\frac{1}{4}$" thickness, and it was coupled with a 5" diameter photomultiplier. The FWHM in pulse height distribution for $^6Li(n,\alpha)T$ reactions peak was about 65 %. The ^7Li glass scintillator (NE906) used for capture gamma ray detection was the same dimensions and the same assembling as that for the ^6Li glass. The photomultiplier tubes were of selected ones for pair wise use. Singnals from these scintillators were pre-amplified and discriminated by timing single channel analysers, inverted, and sent to the TMC-4096 channel time analyser through double shielded baloon type coaxial cables. Most of the electronic circuits were the NIM type JAERI module system. The memory cores of the analyzer were divided into two or four parts, and signals from these detectors were recorded in one of them simultaneously. Neutron flux at the sample position was about $0.1/E^{0.8}$ neutrons per eV per burst for the electron beam of 100 MeV, 0.6 A, and 0.5μsec pulse width. A boron-nitride filter was used to stop the overlapping neutrons of the previous bursts.

Figure 3 shows capture and scattering yields versus time of flight for tungsten plates of three thicknesses in the energy region from 12 to 70 eV. The upper part of the figure are gamma ray yield detected by the ^7Li glass scintillator, and the lower one are scattered neutron yield which are the differences between yield detected by ^6Li glass and that by ^7Li glass. The thicknesses perpendicular to the tungsten plate surface were 0.00016, 0.00248 and 0.0119 atoms/barn, respectively. They were inclined at 45 degree with the

incident beam. Scattered neutrons were detected by the ^{6}Li glass scintiolator which obliquely faced to the incident surface of the samples. For the thinnest sample, capture and scattering yields show peaks at resonance energies as can be seen from fig. 3. However for medium and thick samples these correspondences are degraded; i.e. peaks and dips are inverted in the extreme case. In conclusion following features are found out, and the qualitative interpretations on them are also given.

a) 18.8 eV resonance; Capture gamma ray yield tend to have a constant value just at the resonance energy, that is, peak for thin sample and dip for thick sample. The scattered neutron yields are nearly constant value at the resonance energy.

b) 21.0 and 27.0 eV resonances; Capture gamma ray yields show peaks at somewhat higher side of these resonance evergies, and scattered neutron yields show dips at the same energies. In other words, the thick samples behave like a black absorber for neutrons of these energies.

c) 40.5 eV resonance; Capture gamma ray yields shows a sharp peak and scattered neutron yields shows a small dip which are due to capture of scattered neutrons during passing through deep layer.

These features above are specific for the multiple scattering of neutrons in the samples, and are very difficult to estimate quantitatively by analytical methods.

3. Monte-Carlo Analyses

In order to understand complicated behaviors of the capture and scattering probabilities of neutrons in the thick materials,neutron paths were simulated by the Monte-Carlo method[6] using FACOM 230/60 computor at JAERI.

For an elementary process of scattering and capture between a neutron and a target nucleus, microscopic cross sections were taken into account.

The assumptions on the calculations are as followings.

a) Macroscopic scattering and capture cross sections in energy region of interest are constructed by individual resonance cross sections, each of which is calculated from resonance parameters on the basis of the single level Breit-Wigner formula taking into accounts the Doppler broadening, and the isotopic aboubdances.

b) Reactions other than the capture and elastic scattering are neglected.

c) Isotropic angular distributions for scattering in the center of mass system is assumed.

d) Chemical binding effects are neglected.

e) Motions of target nuclei are neglected.

Outline of the Monte-Carlo calculations are described below.

The mean free path of the neutrons of energy E in the sample is defined by the macroscopic total cross section $\Sigma_t(E)$

$$\lambda(E) = 1/\Sigma_t(E) = 1/(\Sigma_s(E) + \Sigma_c(E)) \quad \text{.....(1)}$$

where $\Sigma_s(E)$, $\Sigma_c(E)$ are the macroscopic scattering and capture cross sections, respectively. For a neutron of energy E_0 incident at P_0 on the surface of the sample, the path length L from P_0 to the first collision point P_1 is determined from a relation

$$L = \lambda(E_0) \log_e(1/(1-YR)) \quad \text{.....(2)}$$

where YR is a uniform random variable of amplitude $0 \leq YR \leq 1$ produced in the program. At the point P_1 either scattering or capture occurs, and the type of the reaction is determined from the value of the subsequent random variable YR; if the value of the YR is less than $\Sigma_s(E_0)/\Sigma_t(E_0)$ the collision is regarded as a scattering, and otherwise it is regarded as a capture. In case of capture, on count is added in the capture counter, and the program returns to the starting point. In case of scattering, the scattering angle θ, ϕ in the center of mass system are determined from the subsequent random variables, and the energy of the

neutron is decreased due to the recoil of the target nucleus to $E_1 = E_0 - E_r$. The recoil energy E_r is given by

$$E_r = 2AE_0(1 - \cos\theta)/(A+1)^2 \qquad \text{.....(3)}$$

where A is the target mass number, and θ is a scattering angle in the center of mass system. The next reaction point P_2 is determined using a new value of $\lambda(E_1)$ in eq.(1), and θ , ϕ transformed into the laboratory system. At the point P_2, type of reactions is determined as done at the point P_1. If the point P_1 or P_2... are out of the sample, one count is added in the escape counter, and the program returns to the starting point. For a capture reaction, number of times of scattering and the sum of path lengthes in the sample for the neutron are recorded. To obtain sufficient statistical accuracy, the number of incident neutrons with a fixed energy is of the order of 1000, in consideration of the computor time.

The geometry of the sample used in the calculations are shown in fig.4. On a disk sample of diameter d and thickness t, neutrons incident at the center of the disk surface. The normal of the disk is inclined with an angle Ψ to the incident neutron direction. In the following analyses it is convenient to classify the neutron paths into five categories. These are,

a) Transmission; penetration through the sample without any interaction in the sample.

b) Front-surface scattering; scattering out from the front surface.

c) Rear-surface scattering; scattering out from the rear surface.

d) Capture in the sample.

e) Side-surface scattering; scattering out from the side surface of the sample.

It is clear that the following relation holds,

$$P_t + P_{fs} + P_{rs} + P_c + P_{ss} = 1 \qquad \text{.....(4)}$$

where P_t, P_{fs}, P_{rs}, P_c, and P_{ss} are the probabilities for the transmission, the front-surface scattering, the rear-surface scattering, the capture, and the side-

surface scattering, respectively. When the sample disk is sufficiently thick and large, the probabilities for the tramsmission, the rear-surface scattering, and the side-surface scattering become very small, and the equation(4) reduces to

$$P_{fs} + P_c \simeq 1 \qquad \text{.....(5)}$$

which means the capture and the front surface scattering probabilities are compliments with each other. Such a case as this occur frequently for neutrons of energy in the resonance region where P_t, P_{rs}, and P_{ss} vanish.

Results of the Monte-Carlo calculations for the capture and the front-surface scattering probabilities of the tungsten plates of several thicknesses are shown in fig.5. Energy region is from 15 to 25 eV, in which two resonances of ^{186}W +n at 18.8 eV and ^{182}W + n at 21.0 eV exist. The tungsten plates are inclined at 45 degrees with the incident beam. The resonance parameters assumed are shown in the figure. In the energy region from 17 to 23 eV, the capture and the front-surface scattering probabilities for the thickest sample share the unity between the two as in a case of eq.(5), since the transmitting neutrons are completely blacked-out in this energy region. Hence the capture and the front-surface scattering probabilities are independent of the sample thickness, but dependent on the cross sections and the recoil energy. The calculated values of these probabilities, normalized to the experimental data are compared with the experimental data. The fitting of the experimental data in fig.3 to the calculated curve in fig.5b are shown in fig.6, in the energy region from 15 to 30 eV. The fitting is generally good, except for scattering yield in the energy region below 15 eV and capture yield for higher energy side of the 21.0eV resonance. For the 27-eV resonance of ^{183}W + n, the reason for rather a large value of experimental capture yield is considered to be due to relatively intense capture gamma rays of high energy than those of resonances of even isotopes ^{182}W

and ^{186}W. These high energy gamma ray components are preferably detected with the present Li glass scintillator and pulse height discrimination system.
Figure 7 shows comparison of observed rear-surface scattering and capture yields with the calculated curves for 18.8, 21.0, and 27.0 eV resonances. The fitting is fairly good.

In order to obtain more clear picture of the multiple scattering effect, path lengths of the incident neutrons in the sample are analysed by the Monte-Carlo method. In the figure 8, distribution of path length of neutron in the sample until they are captured is shown. The sample is a tungsten plate of 1 mm thickness and 10 cm diameter inclined at 45 degrees to the incident beam.
The incident energy is varied from 15 to 28 eV, and the capture probabilities for neutron path length are shown as functions of the path length in every interval of 0.1 mm width. From the figure 8, we see charactaristic features for the neutron capture taking place in thick resonance materials. When the incident neutron energy is equal to a resonance energy, a large portion of the capture event occurs at the surface region simply because at this energy the neutron has a very short mean free path. As the scattering cross section is also large at this energy, reflection of the incident neutron at the surface limits the maximum value of the capture probability in the sample. For either side of the resonance energy, mean free path is not so short, and the neutron permeates rather deeply into the sample. So the capture probability summed over all the volume in the sample can be larger than that just at the resonance energy, where a large portion of capture events takes place at the surface layer. This phenomenon does not occur in case of a very thin sample of which thickness is less than the mean free path of the neutrons even at resonance energies, and it occurs more or less for sufficiently thick samples.
In the off-resonance region, mean free path become longer than the present

sample thickness, and the neutrons permeate rather uniformely throughout the sample as shown in the figure 8 in the region from 15 to 17 eV and from 23 to 26 eV, respectively.

Capture and front-surface scattering probabilities of metallic cobalt plates are calculated and shown in fig.9 in the energy region from 100 to 180 eV, where a 132 eV resonance exists. Resonance parameters used are also shown in the figure. Saturation of capture probabilities at the resonance energy is noted. Figure 10 shows calculated probabilities of neutron capture for 5.2 eV resonance in natural silver for neutrons impinge perpendicularly on the sample. For thick silver samples, the capture probabilities just at the 5.2-eV resonance have a tiny dip at the top of the capture probability distribution.

4 Saturated Values of Capture Probabilities at Resonance

The value of capture probabilities at resonance are saturated as the sample thickness increase sufficiently, and are denoted as P_{c0}. The values of P_{c0} are equal to 0.38 for the 18.8-eV resonance in tungsten, 0.22 for the 132-eV resonance in cobalt, and 0.98 for the 5.2-eV resonance in silver as shown in fig.5,9, and 10. It is important to find out relations between resonance parameters and P_{c0}. By the Monte-Carlo method the saturated values of capture probabilities at resonance P_{c0} were calculated as functions of Γ_n/Γ with different sets of parameter Γ/E_r, where $E_r = 2AE/(A+1)^2$ a measure of recoil energy, and Γ the total width of the resonance. In case of $\Gamma_\gamma \gg \Gamma_n$ or $\Gamma_n/\Gamma \ll 1$, an incident neutron is preferably captured and P_{c0} become a value near the unity, whereas in cace of $\Gamma_\gamma \ll \Gamma_n$ or $\Gamma_n/\Gamma \simeq 1$ an incident neutron is preferably scattered out from the sample, and P_{c0} become a small value. The meaning of the parameter Γ/E_r is following. In a collision with a target nucleus of mass A,

a neutron losses recoil energy of which average is E_r. In multiple scattering of a neutron in the sample, Γ/E_r is the average number of collisions, in between the neutron possesses its energy which is in the resonance region of target nucleus.

Figure 11 shows relation between P_{c0} and Γ_n/Γ with 5 sets of parameters Γ/E_r, obtained by the Monte-Carlo method, where points A,B,C,and D in the figure correspond to real resonances in tungsten(18.8,27.0 eV), cobalt(132 eV), and silver(5.2 eV). For a resonance of constant energy, it is found that P_{c0} does not change so much as long as Γ_n/Γ and Γ/E_r are constant, though the Γ_n and Γ values change for more than a factor of 10.

Energy dependence of P_{c0} are shown in fig.12 where resonance parameters other than resonance energy are constant. It is noted that P_{c0} are rather slowly varing functions of resonance energy, though the peak cross sections of the resonance varies propotional to $2.6 \times 10^6/E$ (barn) where E is resonance energy in eV.

These facts show rather direct dependence of P_{c0} on Γ_n/Γ. From the results shown in fig.11 and 12, rough value of Γ_n/Γ can be obtained when the value P_{c0} are experimentally observed for resonances. This will be a new method of Γ_n/Γ estimation which is essentially insensitive to the sample thickness when it is sufficiently thick. However, the accuracy in Γ_n/Γ such obtained is not so good , when Γ/E_r is not known. To obtain more accurate value of Γ_n/Γ, another value of resonance parameter,for example Γ_n, is needed. When the values of P_{c0}, E_r and Γ_n are known for a resonance, Γ value can be obtained on the curves in fig.11. However, the accuracy in Γ value such obtained will not be so good for small value of Γ_n/Γ, as can be seen in fig.11.

The author wishes to thank to Dr.Takekoshi and Dr.Asami for the support of this work, and to Dr. Nishimura for reading the manuscript.

References

1) J.E.Lynn; The Theory of Neutron Resonance Reactions
Clerendon Press (1968) p 32

2) F.H.Fröhner; GA-6909 (1966)

3) H.Takekoshi et al.; JAERI-1238 (1975)

4) M.Ohkubo ; JAERI-M 5624 (1974)

5) M.Asgher and F.D.Brooks; Nucl.Instr.Methods 39(1966)68

6) T.Nakayama and O.Miyatake; Monte-Carlo Method (1960)Nikkan Kogyo Press

Figure Captions

Fig.1 Schematic figure of the time of flight facilities at JAERI linac.

Fig.2 Constructions of the scattering and capture detectors.

Fig.3 The upper figure shows observed neutron capture gamma ray yields for tungsten plates of three thicknesses measured by ^{7}Li glass scintillator, and the lower figure shows corresponding scattered neutron yields measured by the ^{6}Li glass subtracted off the gamma ray components. The samples were plates of 0.000164,0.00248, and 0.0119 atoms/barn respectively, inclined at 45 degrees with the incident beam. Channel width was 0.5 sec/channel.

Fig.4 Geometry of the sample for Monte-Carlo calculations.

Fig.5a Capture and front-surface scattering probabilities of tungsten plates in energy region from 15 to 25 eV calculated by the Monte-Carlo method, with conditions shown in the figure.

Fig.5b Capture and front-surface scattering yield for tungsten plates. These curves are obtained by normalizing the curves in fig.5a to fit the present time-of-flight experimental data.

Fig.6 Neutron capture and front-surface scattering yields in the energy region from 15 to 30 eV. Observed data and calculated curves are shown.

Fig.7 Neutron capture and rear-surface scattering probabilities of tungsten in the same energy region as in the fig.6. Observed data and calculated curves are shown.

Fig.8 Distributions of path lengthes of neutrons until they are captured in a tungsten plate of 1 mm thickness inclined at 45 degrees with the incident beam. The capture probabilities for neutron path length are shown as functions of the path length in every interval of 0.1 mm width.

Fig.9 Calculated capture and front-surface scattering probabilities of metallic cobalt plates of several thicknesses. Saturated dip in capture

probabilities at resonance is noted.

Fig.10 Calculated capture probabilities of metallic silver plates of several thicknesses around 5.2 eV resonance. Saturated dip is observed at the top of the capture peak.

Fig.11 Saturation values of capture probabilities at resonance P_{c0} as functions of Γ_n/Γ with parameters of Γ/E_r.

Fig.12 Saturation values of capture probabilities at resonance P_{c0} for a separated resonance having constant total width Γ = 6.0 eV. Resonance energies are varied from 10 to 1320 eV, for several value of Γ_n/Γ .

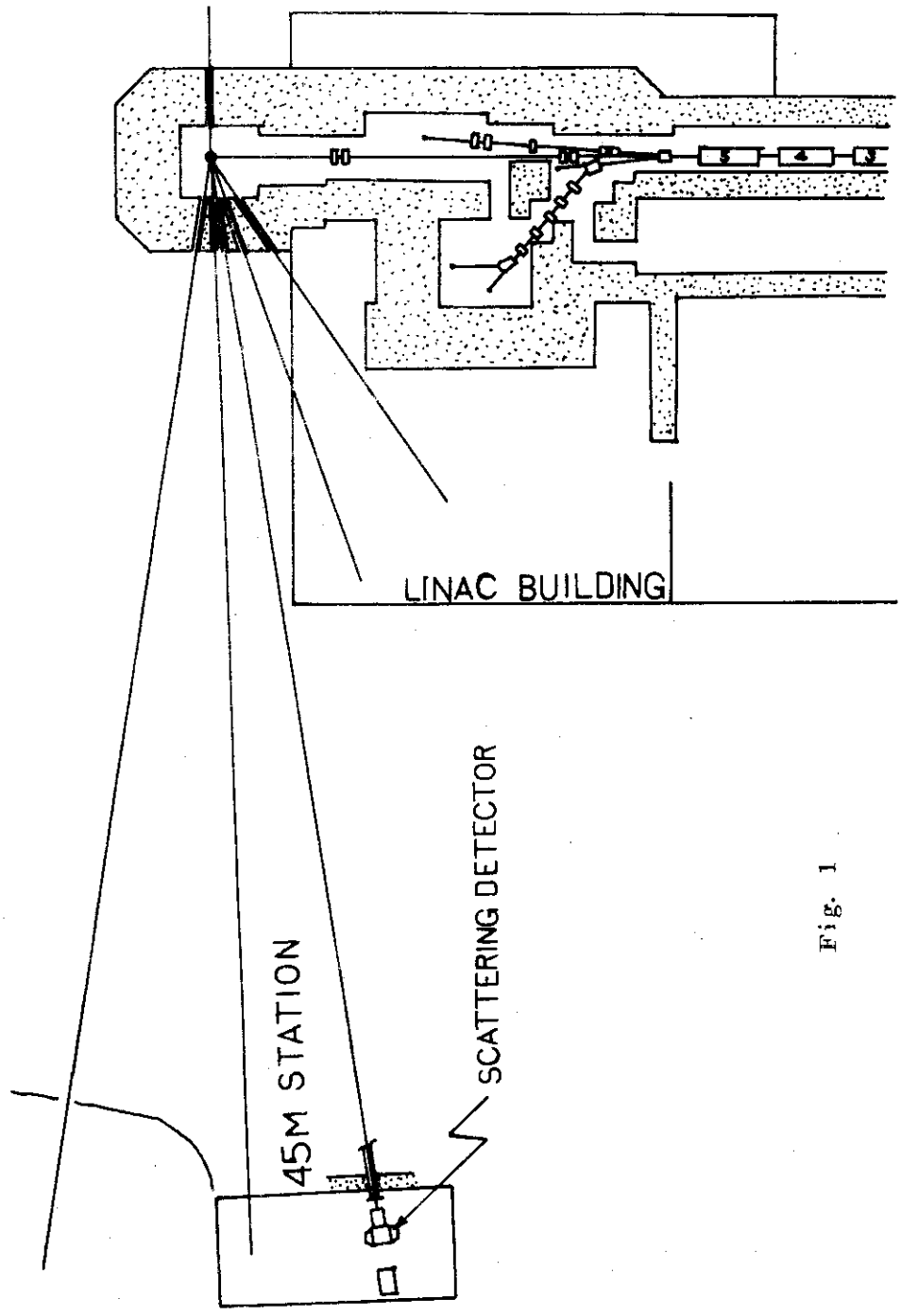

Fig. 1

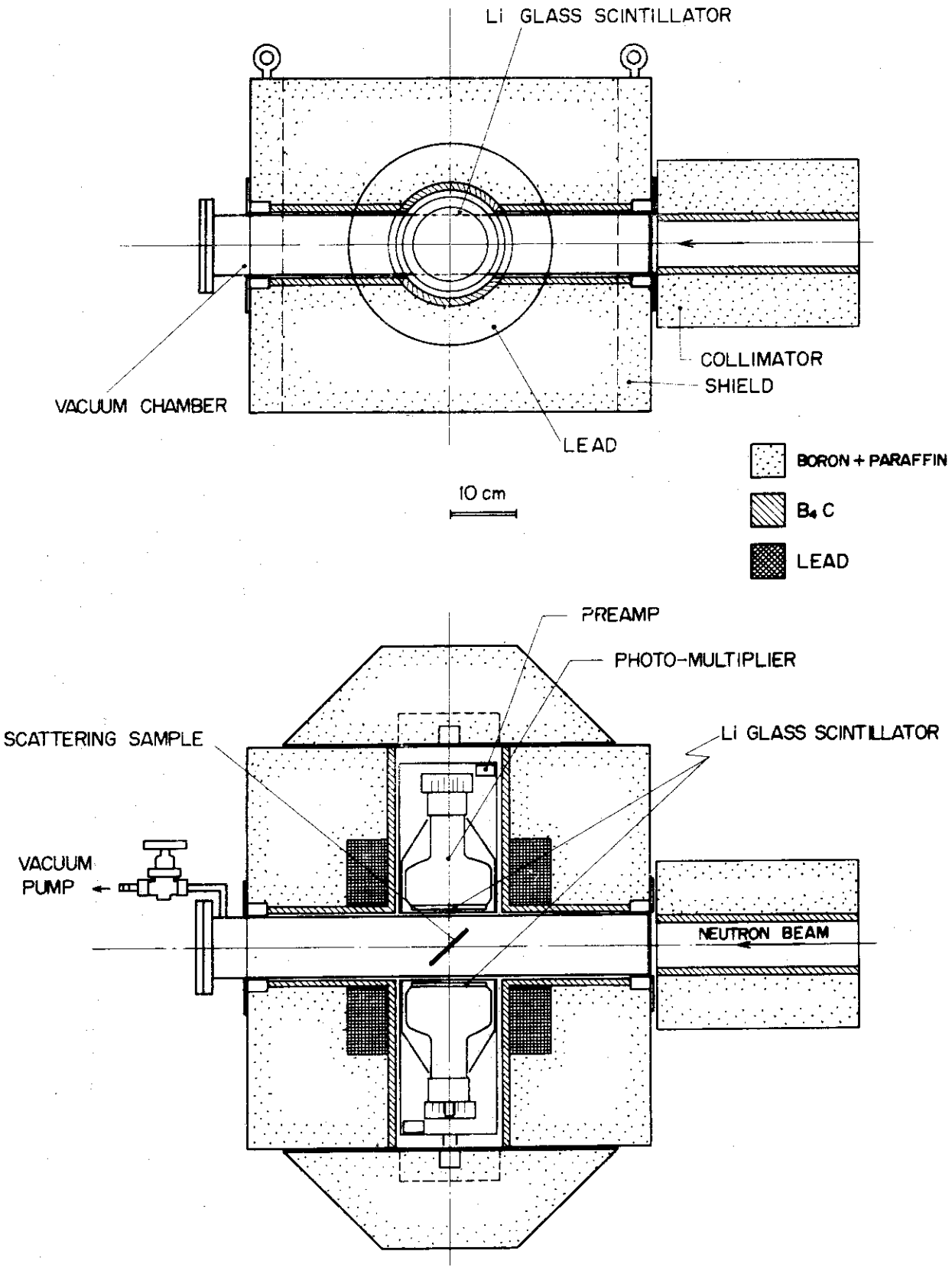
Li GLASS SCINTILLATOR
VACUUM CHAMBER
LEAD
COLLIMATOR
SHIELD
10 cm
BORON + PARAFFIN
B_4C
LEAD
PREAMP
PHOTO-MULTIPLIER
SCATTERING SAMPLE
Li GLASS SCINTILLATOR
VACUUM
PUMP
NEUTRON BEAM

Fig. 2

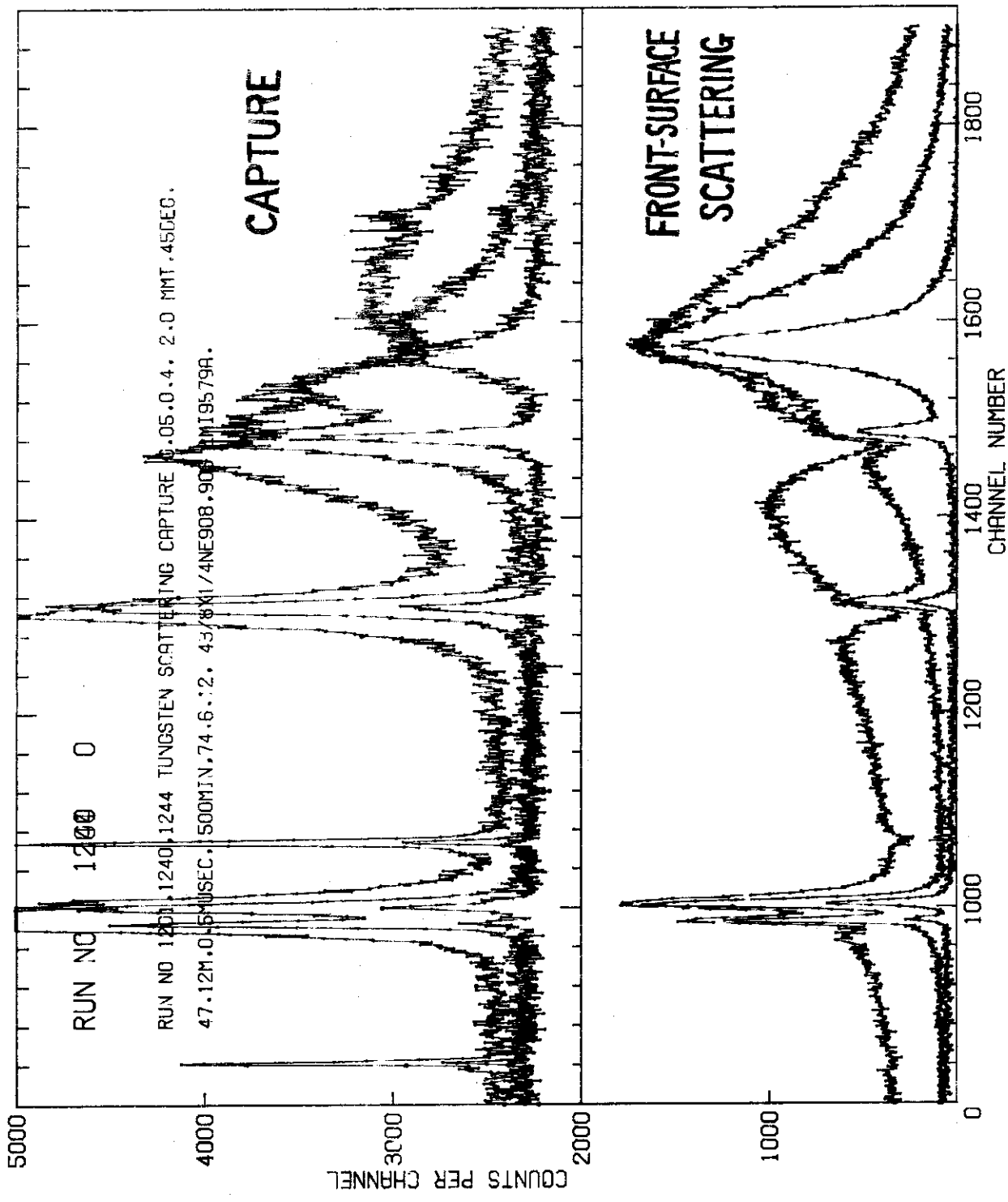
CAPTURE
FRONT-SURFACE SCATTERING
COUNTS PER CHANNEL
CHANNEL NUMBER
5000
4000
3000
2000
1000
0
1000
1200
1400
1600
1800
RUN NO 1200 0
RUN NO 1200,1240,1244 TUNGSTEN SCATTERING CAPTURE 6.05.0.4. 2.0 MMT.45DEG.
47.12M.0.5MUSEC, 500MIN,74.6.12. 43/8K1/4NE908,90 MM19579A.

Fig. 3

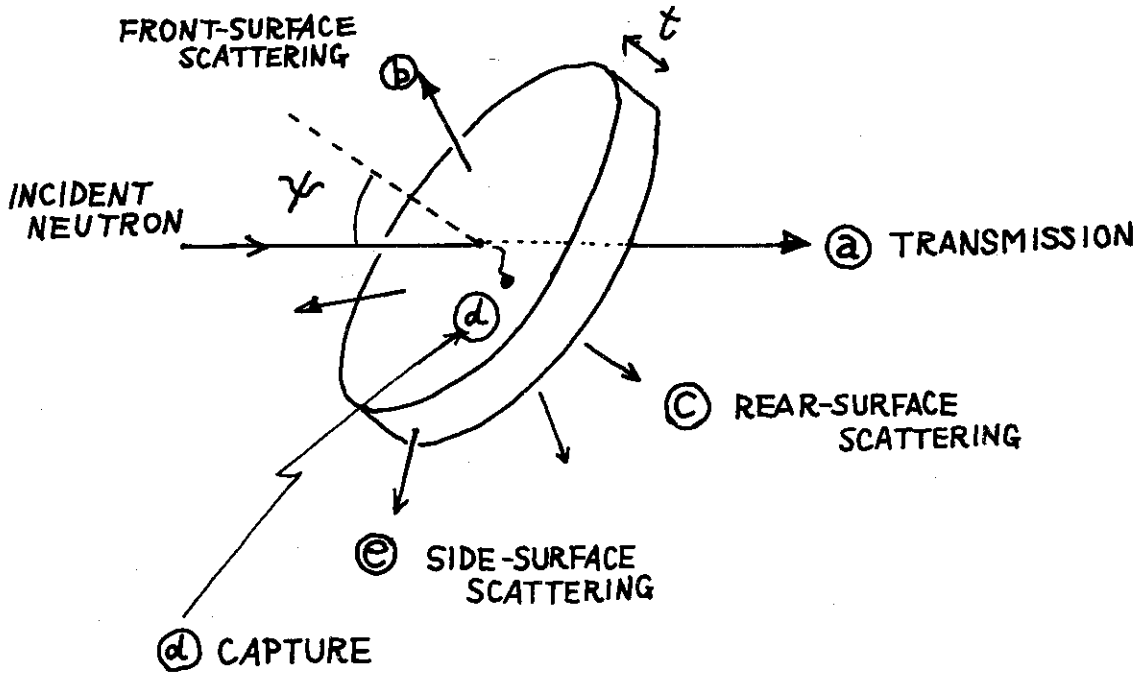
FRONT-SURFACE SCATTERING
b
t
INCIDENT NEUTRON
γ
a TRANSMISSION
d
C REAR-SURFACE SCATTERING
e SIDE-SURFACE SCATTERING
d CAPTURE

Fig. 4

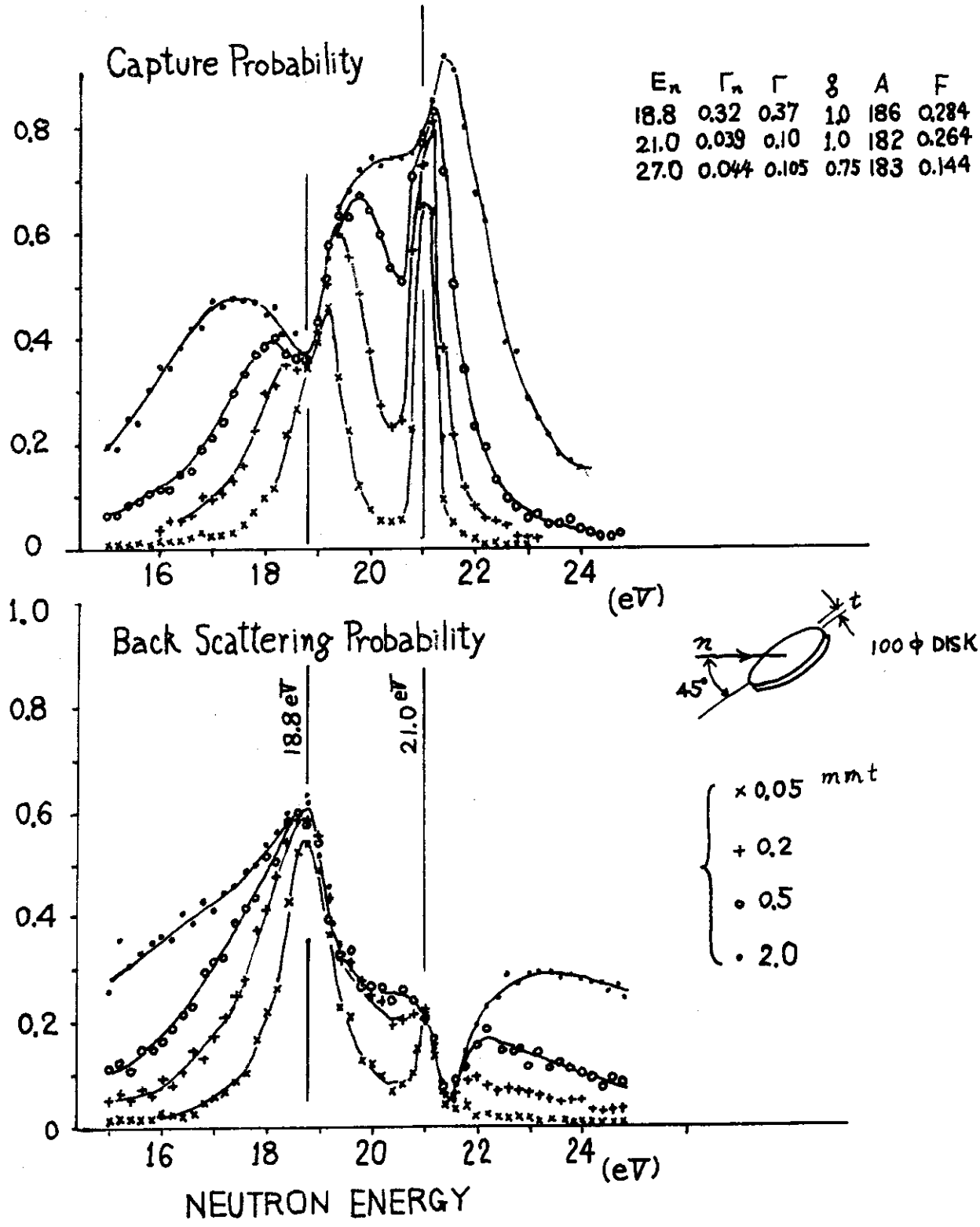
Capture Probability
E_n Γ_n Γ g A F
18.8 0.32 0.37 1.0 186 0.284
21.0 0.039 0.10 1.0 182 0.264
27.0 0.044 0.105 0.75 183 0.144
0.8
0.6
0.4
0.2
0
16 18 20 22 24 (eV)
Back Scattering Probability
18.8eV
21.0eV
1.0
0.8
0.6
0.4
0.2
0
16 18 20 22 24 (eV)
NEUTRON ENERGY
t
n
45°
100φ DISK
× 0.05 mmt
+ 0.2
∘ 0.5
• 2.0

Fig. 5 a

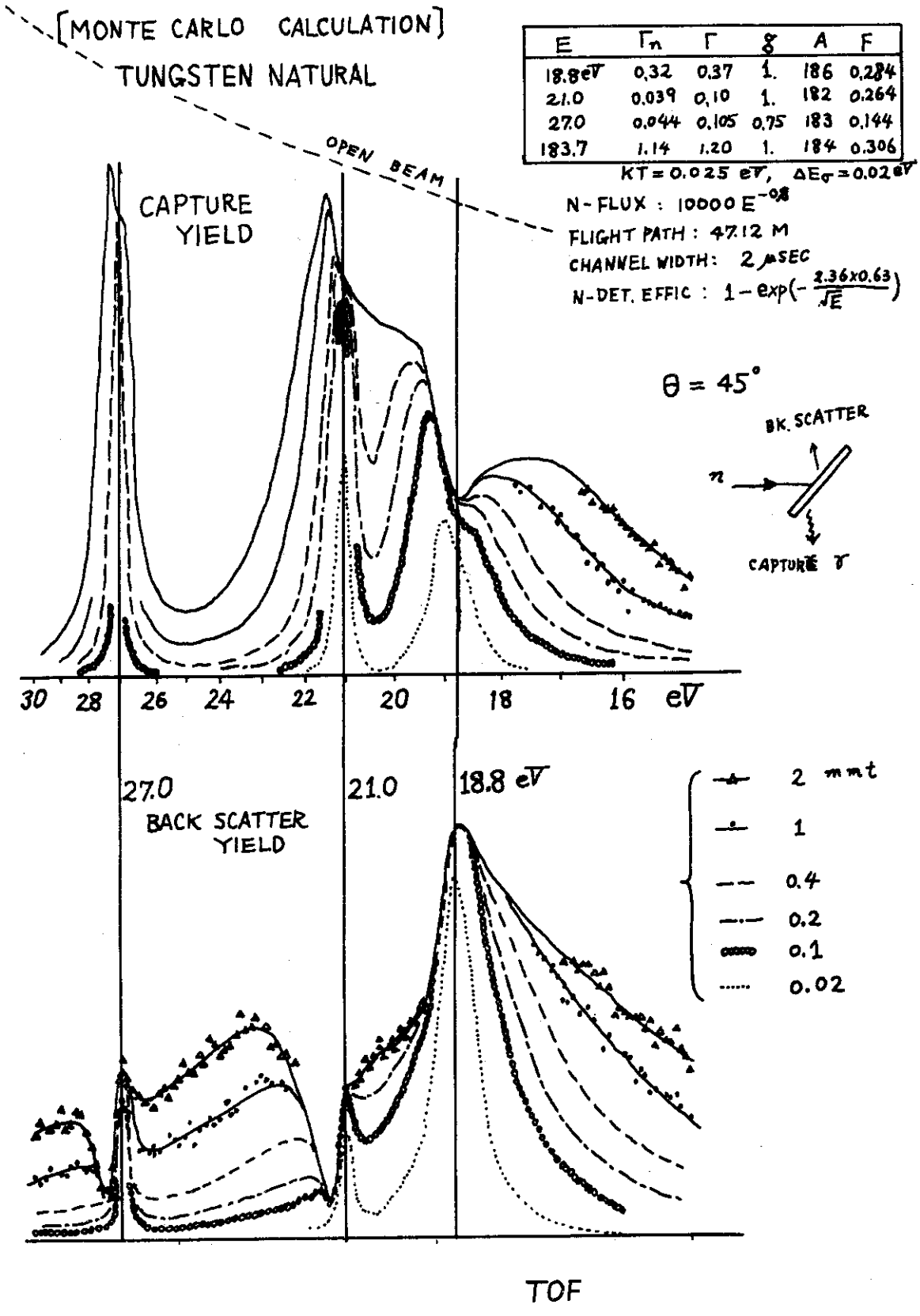

E	Γ_n	Γ	g	A	F
18.8eV	0.32	0.37	1.	186	0.284
21.0	0.039	0.10	1.	182	0.264
27.0	0.044	0.105	0.75	183	0.144
183.7	1.14	1.20	1.	184	0.306

KT = 0.025 eV, ΔE_σ = 0.02 eV

Fig. 5 b

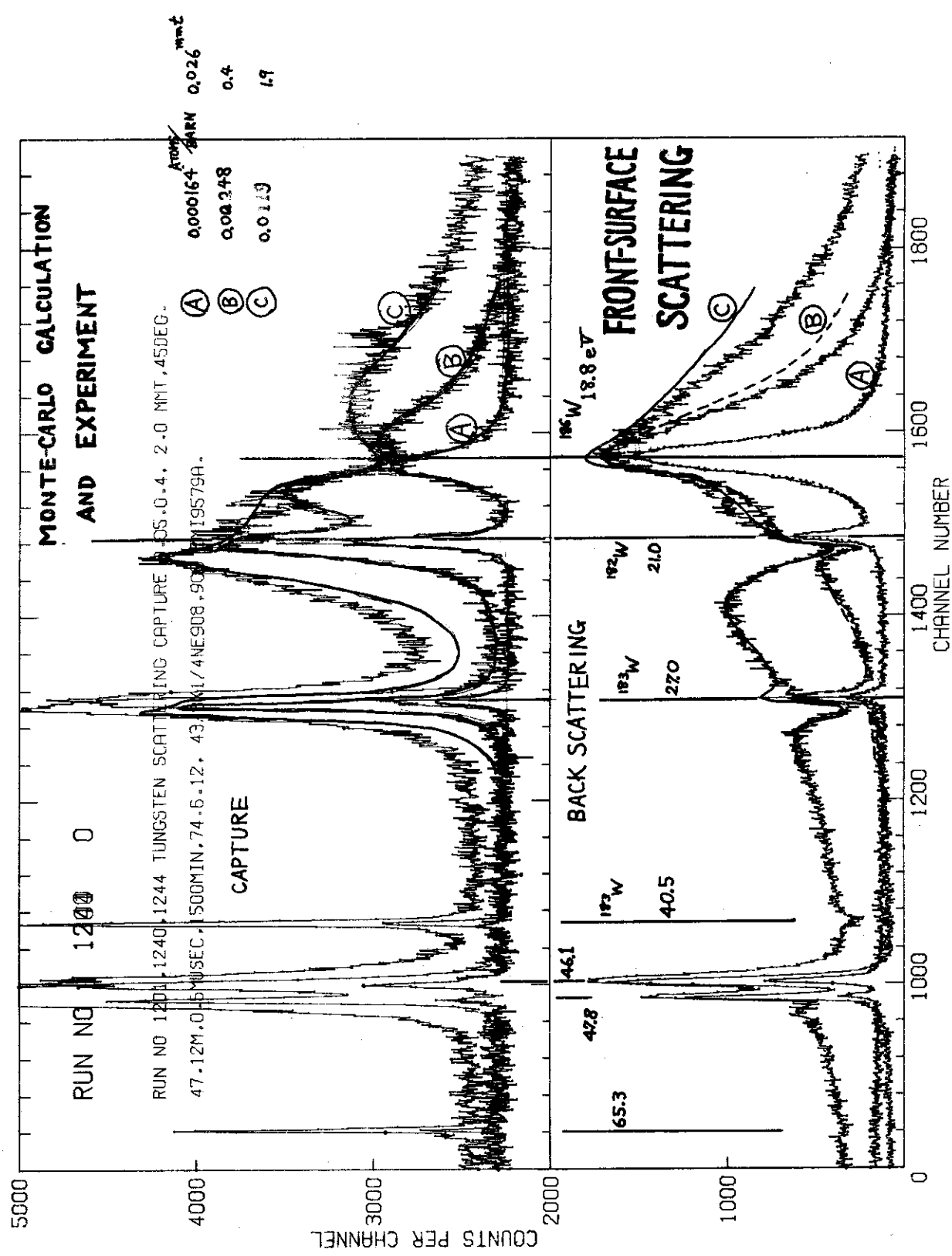
MONTE-CARLO CALCULATION
AND EXPERIMENT
RUN NO 1201 1240 1244 TUNGSTEN SCATTERING CAPTURE
47.12M,0.6MUSEC,1500MIN,74.6.12, 43
CAPTURE
A 0.000164 ATOM/BARN 0.026 mmt
B 0.00348 0.4
C 0.0113 1.9
^{186}W 18.8 eV
FRONT-SURFACE SCATTERING
BACK SCATTERING
^{182}W 21.0
^{183}W 27.0
^{183}W 40.5
46.1
47.8
65.3
COUNTS PER CHANNEL
CHANNEL NUMBER
0
1000
2000
3000
4000
5000
1200
1400
1600
1800

Fig. 6

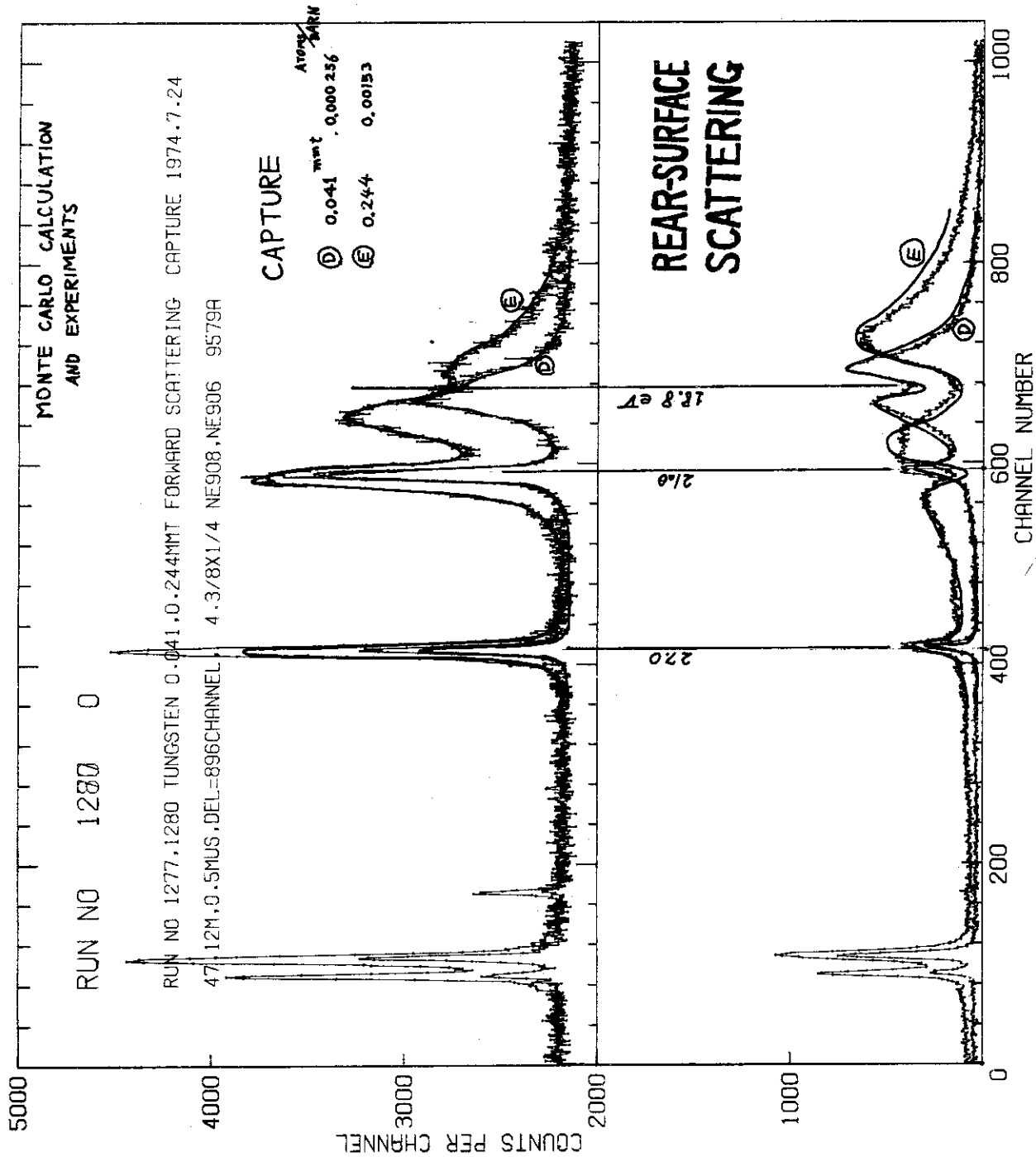
MONTE CARLO CALCULATION
AND EXPERIMENTS
RUN NO 1280 0
RUN NO 1277,1280 TUNGSTEN 0.041,0.244MMT FORWARD SCATTERING CAPTURE 1974.7.24
47,12M,0.5MUS,DEL=896CHANNEL, 4.3/8X1/4 NE908,NE906 9579A
CAPTURE
D 0.041 mmt 0.000256 Atoms/BARN
E 0.244 0.00153
REAR-SURFACE
SCATTERING
270
2.0
18.8 eV
COUNTS PER CHANNEL
CHANNEL NUMBER
5000
4000
3000
2000
1000
0
200
400
600
800
1000

Fig. 7

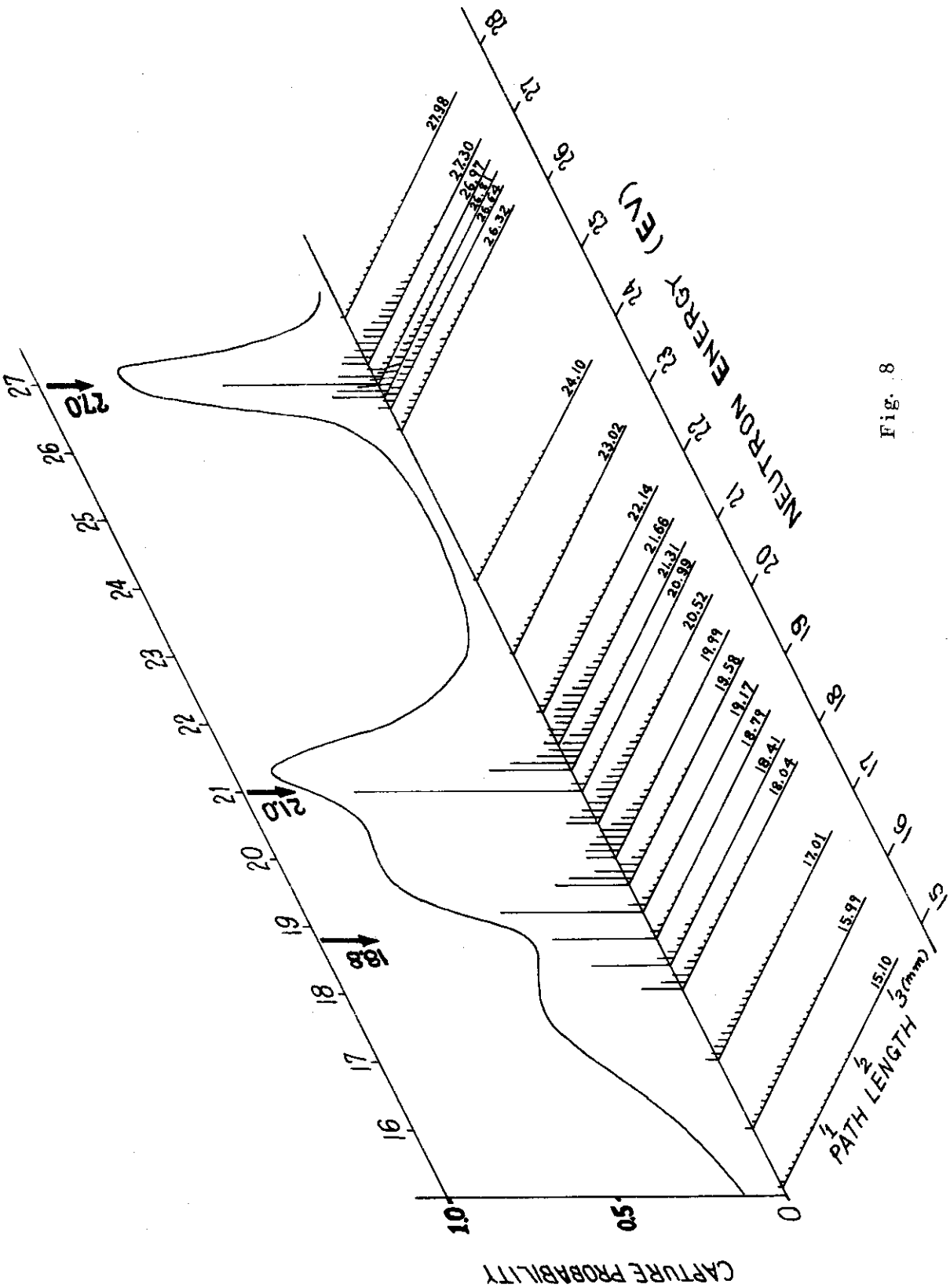
CAPTURE PROBABILITY
1.0
0.5
0
PATH LENGTH
1/4
1/2
3/4
(mm)
15.10
15.91
17.01
18.04
18.41
18.78
19.17
19.58
19.99
20.52
20.99
21.31
21.66
22.14
23.02
24.10
26.32
26.64
26.97
27.30
27.98
NEUTRON ENERGY (EV)
27
26
25
24
23
22
21
20
19
18
17
16
15
14
13
12
11
10
9
8
7
6
5
4
3
2
1
27.0
21.2
18.8

Fig. 8

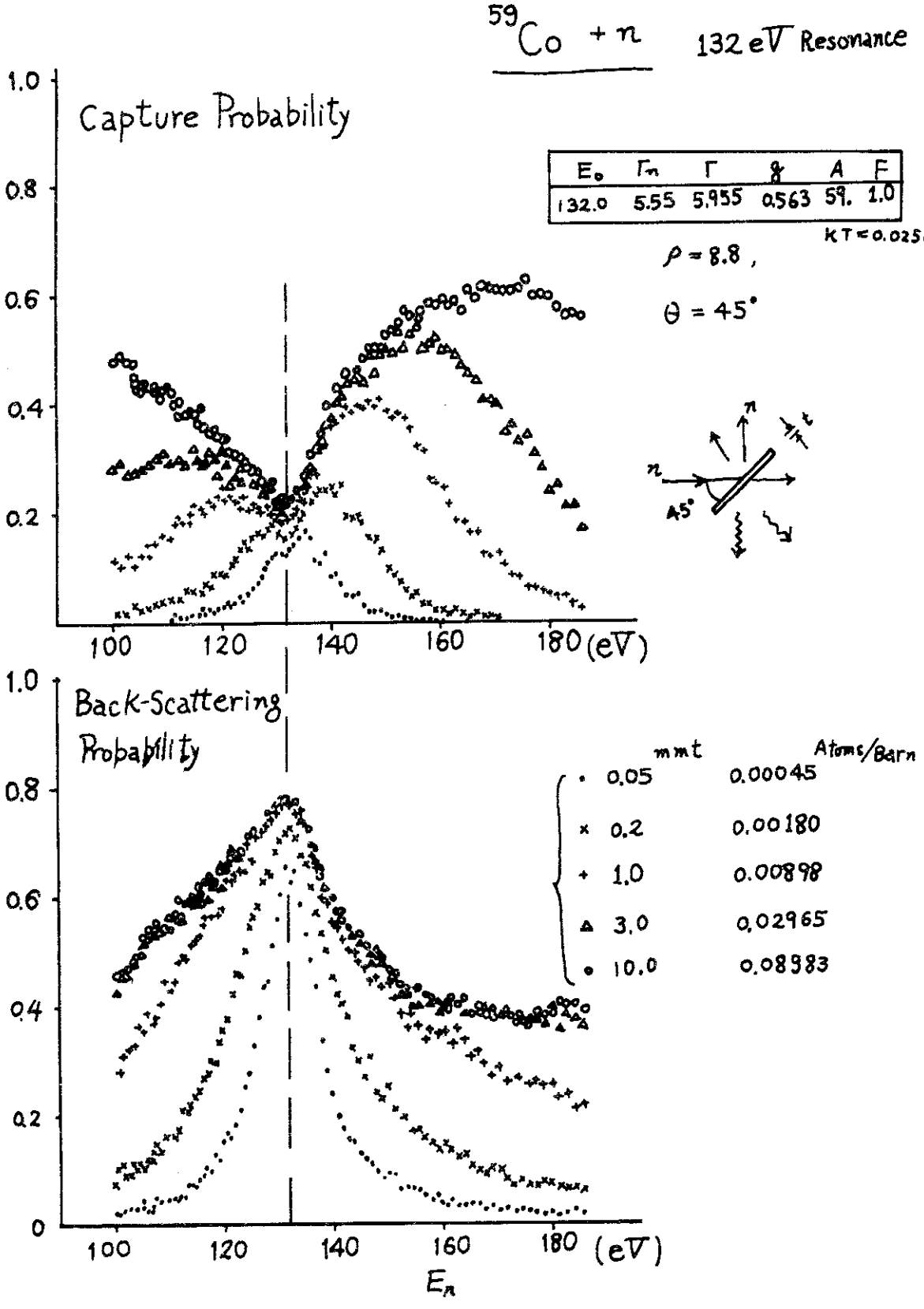
59Co + n 132 eV Resonance
Capture Probability
Back-Scattering Probability
E0 Γn Γ g A F
132.0 5.55 5.955 0.563 59. 1.0
kT=0.025eV
ρ = 8.8,
θ = 45°
45°
mmt Atoms/Barn
0.05 0.00045
0.2 0.00180
1.0 0.00898
3.0 0.02965
10.0 0.08983
1.0
0.8
0.6
0.4
0.2
0
100 120 140 160 180 (eV)
En

Fig. 9

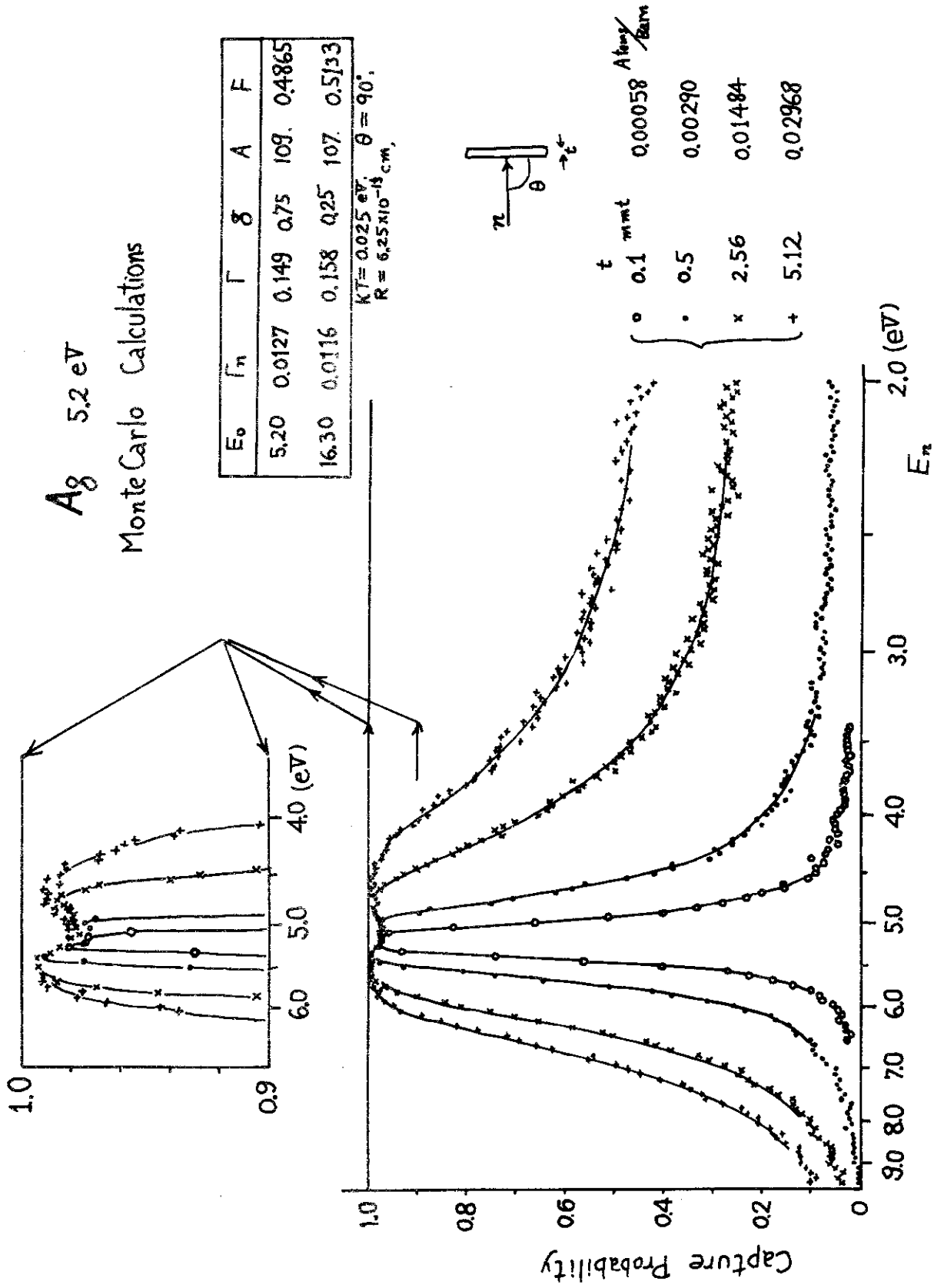
A_8 5.2 eV
Monte Carlo Calculations
E_0 Γ_n Γ δ A F
5.20 0.0127 0.149 0.75 109. 0.4865
16.30 0.0116 0.158 0.25 107. 0.5133
KT= 0.025 eV, θ = 90°,
R = 6.25×10⁻¹³ cm,
t
° 0.1 mmt 0.00058 Atom/Barn
• 0.5 0.00290
× 2.56 0.01484
+ 5.12 0.02968
n
θ
t
Capture Probability
E_n
2.0 (eV)
3.0
4.0
5.0
6.0
7.0
8.0
9.0
0
0.2
0.4
0.6
0.8
1.0
4.0 (eV)
5.0
6.0
0.9
1.0

Fig. 10

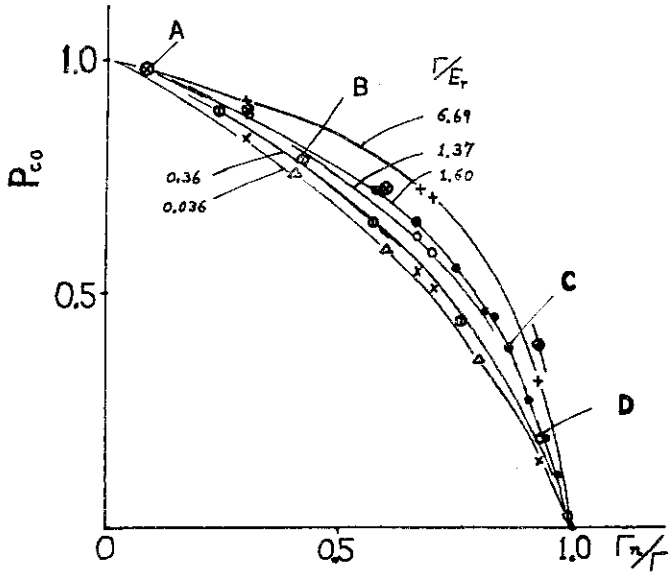

		E_0	Γ_n	Γ	g	F	E_r	Γ/E_r
A	^{109}Ag	5.2 eV	0.0127	0.149	0.75	0.486	0.093	1.62
B	^{183}W	27.0	0.044	0.105	0.75	0.144	0.294	0.36
C	^{186}W	18.8	0.32	0.37	1.0	0.284	0.200	1.60
D	^{59}Co	132.	5.55	5.95	0.563	1.0	4.33	1.37

Fig. 11

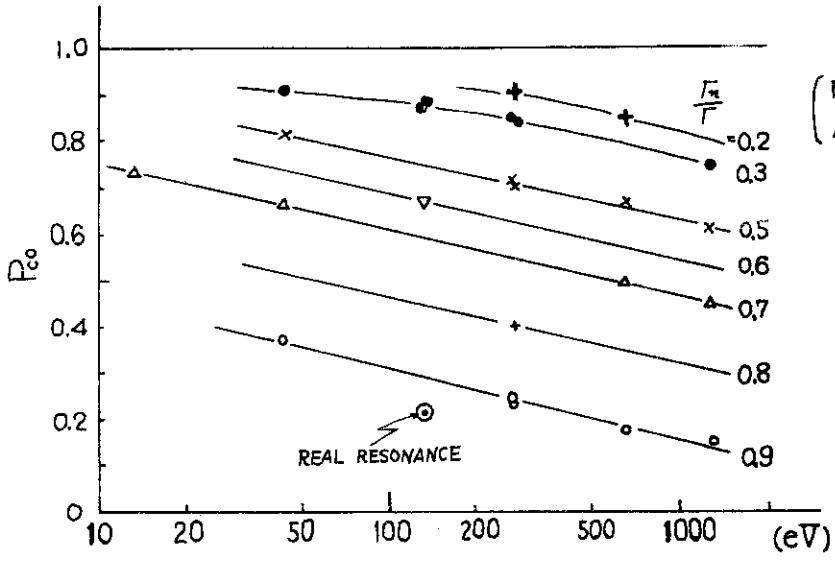

REAL RESONANCE

E_0 eV	Γ_n	Γ	g	A	F	Γ_n/Γ
132	5.55	5.955	0.563	59	1.0	0.93

Fig. 12